Modeling acoustic resonators using higher-order equivalent circuits

Caleb B. Goates[a)], Matthew F. Calton[b)], Scott D. Sommerfeldt[c)] and David C. Copley[d)]

(Received: 17 April 2019; Revised: 17 October 2019; Accepted: 18 October 2019)

Helmholtz resonators are widely used, but classical models for the resonators, such as the lumped-element equivalent circuit, are inaccurate for most geometries. This article presents higher-order equivalent circuits for describing the resonators based on the one-dimensional wave equation. Impedance expressions are also derived. These circuits and expressions are given for various constituent resonator components, which may be combined to model resonators with curved, tapered, and straight necks. Resonance frequency predictions using this theory are demonstrated on two realistic resonators. The higher-order predictions are also applied to the theory of side branch attenuators in a duct and the theory of resonator coupling with a mode of an enclosure. © *2019 Institute of Noise Control Engineering.*

Primary subject classification: 34.3; Secondary subject classification: 76.9

1 INTRODUCTION

A Helmholtz resonator consists of an enclosed volume, or cavity, with a hole or neck of finite length. Helmholtz resonators are well-known and effective noise control devices, but classical formulations for predicting their response often prove inaccurate for all but the most simplistic and ideal geometries. Typically, these resonators are used to attenuate tonal noise in pipes or ducts, damp
R1 modes in enclosures[1], and increase transmission loss
R2 through a partition[2]. Once tuned, Helmholtz resonators can often be forgotten, as they need very little maintenance. The Helmholtz resonator is characterized by a large attenuation over a narrow bandwidth; hence, tuning is critical in many single-resonator applications. Unfortunately, classical expressions for resonator properties compromise accuracy for simplification. Resonance frequency predictions, for example, can yield errors of 10%–30% for non-ideal
R3 resonators[3]. In addition, ideal geometry resonators are rarely used in industrial applications, as compactness and manufacturability often constrain the design. As a result, unconventional neck geometries and volume shapes may be employed in practical resonator designs. In practice, the tuning problem is usually solved by repeated resonator prototyping, which can delay project schedules and increase costs.

Much previous work has attempted to compensate for these inaccuracies. The classical formulation for the resonance frequency has changed little since it was presented by Rayleigh in 1870[4], but several corrections to the for- **R4**
mula have been developed. These include accounting for inaccuracies using end corrections[5,6], by calculating **R5 R**
the total acoustic mass using velocity field lines[3], or by developing specialized expressions for pancake or long resonators[7]. The regularity of publications on the Helmholtz **R7**
resonator indicates a need for more robust and flexible formulations, which account for many current and future resonator designs. Some more recent efforts employ finite element or boundary element analysis; these methods accurately predict resonance frequencies, albeit at the cost of computational efficiency and design flexibility.

One modeling method that is computationally efficient but has found limited application to resonators is the equivalent circuit. Equivalent circuits as used in this article treat volume velocity as an electric current and acoustic pressure as a voltage and allow acoustic systems to be represented by electrical circuits. Circuit representations allow construction of systems of equations by inspection[8]. They **R8**
also make available a century's worth of circuit analysis techniques, including, for example, the use of circuit loops to quickly construct a system matrix equation. It is common to represent the Helmholtz resonator with a lumped-element circuit, where low-frequency effects are described using equivalent inductance, capacitance, and resistance elements. This approach can be found in many introductory acoustics textbooks. Lumped elements are an approximation, however, which is valid only when all dimensions are much less than a wavelength, and in practice, they

a) Department of Physics and Astronomy, Brigham Young University; N283 ESC, Provo, UT 84602, USA; email: calebgoates@gmail.com

b) Department of Physics and Astronomy, Brigham Young University, N283 ESC, Provo, UT 84602, USA; email: mattcalton@gmail.com

c) Department of Physics and Astronomy, Brigham Young University; N283 ESC, Provo, UT 84602, USA; email: scott_sommerfeldt@byu.edu

d) Caterpillar Inc., Technical Center, Bldg E-557, 14009 Old Galena Road, Mossville, IL 61552, USA; email: copley_david_c@cat.com.

exhibit the inaccuracies described above. Though higher-order circuits have long been implemented in transducer analysis[8], speech production modeling[9], and other areas of acoustics, to the knowledge of the authors, no published effort exists to describe the Helmholtz resonator using higher-order circuits.

The approach presented here uses one-dimensional solutions to the wave equation to create equivalent circuits and impedance expressions. This relaxes the lumped-element requirement of all dimensions being small compared to a wavelength, as systems may be distributed along one dimension. Equivalent circuits are developed for constituent components of resonators and then combined to model a complete resonator. In addition to the equivalent circuits, this article will develop expressions for the input impedance at one end of a constituent component in terms of the impedance attached to the other end. These alternate formulations, termed impedance translation expressions, can also be combined to model the entire resonator, and may be useful if the only quantity of interest is the input impedance.

2 THEORY

The following theoretical discussion introduces three types of equivalent circuits. First, waveguides are modeled as equivalent circuits with two pairs of terminals, one pair representing each end of the guide. This type of circuit is developed for straight, curved, and tapered waveguides. Second, resonator cavities are modeled as a terminating impedance. Third, end corrections are modeled as either a series impedance element or an additional waveguide length.

2.1 Waveguides

A one-dimensional waveguide has a definition of both acoustic pressure and volume velocity at each end (see Fig. 1(a)) and therefore should be modeled as a two-terminal-pair equivalent circuit. These circuits are also referred to as two-ports, with a port being a pair of terminals with a defined voltage and current. One simple two-port circuit is the T-network[10], which is shown in Fig. 1(b). A T-network includes three impedance elements, which may have arbitrary impedance expressions. For the purposes of resonator design, the T-network offers a means by which the wave effects of an acoustic waveguide can be modeled as an equivalent electrical circuit. The expressions for the relevant impedance elements can be derived using the general solution of the pressure and volume velocity in the waveguide, as follows: the one-dimensional waveguide can be described by the 1D wave equation, or by the 1D Helmholtz equation if $e^{j\omega t}$ time dependence is assumed, where $j = \sqrt{-1}$, ω is the angular frequency, and t is time.

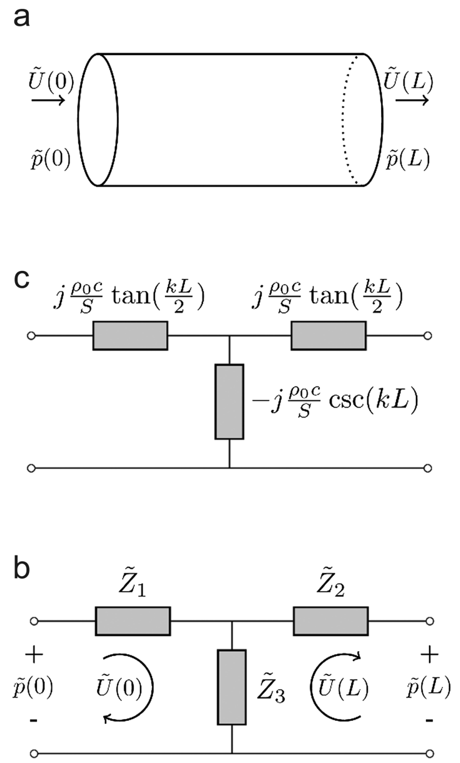

Fig. 1—An illustration of the equivalent circuit development for a straight waveguide. (a) The waveguide, with the pressure and volume velocity at each end defined. (b) The general form of the equivalent circuit for a waveguide. (c) The fully developed equivalent circuit for a straight waveguide.

The general solution to the latter differential equation is

$$\widetilde{p}(x) = C_1 e^{jkx} + C_2 e^{-jkx}, \qquad (1)$$

where k is the wavenumber, x is the spatial dimension along the length of the waveguide, and C_1 and C_2 are arbitrary constants. The general solution for the volume velocity $U(x)$ can be found using Euler's equation,

$$\widetilde{U}(x) = \frac{jS}{\rho_0 \omega}\frac{d\widetilde{p}}{dx} = -\frac{S}{\rho_0 c}\left[C_1 e^{jkx} - C_2 e^{-jkx}\right], \qquad (2)$$

where ρ_0 is the ambient density of air, c is the speed of sound, and S is the cross-sectional area of the waveguide. The impedance expressions are then found by evaluating these general solutions with various boundary conditions, as follows:

$$\widetilde{Z}_3 = \left.\frac{\widetilde{p}(L)}{\widetilde{U}(0)}\right|_{\widetilde{U}(L)=0}, \qquad (3a)$$

$$\widetilde{Z}_1 + \widetilde{Z}_3 = \left.\frac{\widetilde{p}(0)}{\widetilde{U}(0)}\right|_{\widetilde{U}(L)\,=\,0}, \tag{3b}$$

$$\widetilde{Z}_2 + \widetilde{Z}_3 = \left.\frac{\widetilde{p}(L)}{\widetilde{U}(L)}\right|_{\widetilde{U}(L)\,=\,0}, \tag{3c}$$

where $\widetilde{Z}_1$, $\widetilde{Z}_2$, and $\widetilde{Z}_3$ are as indicated in Fig. 1(b), and L is the length of the waveguide. Substituting Eqns. (1) and (2) into Eqns. (3a)–(3c) and simplifying give the expressions for the T-network elements of a straight waveguide, which are present in the literature:

$$\begin{aligned}\widetilde{Z}_{1,\text{straight}} &= \widetilde{Z}_{2,\text{straight}} = j\frac{\rho_0 c}{S}\tan\left(\frac{kL}{2}\right), \widetilde{Z}_{3,\text{straight}} \\ &= -j\frac{\rho_0 c}{S}\csc(kL).\end{aligned} \tag{4}$$

The completed straight waveguide circuit with the impedance expressions included is shown in Fig. 1(c). The treatment of the other waveguides in this article is carried out in a similar manner; Eqns. (3a)–(3c) are general, while Eqns. (1) and (2) are specific to the straight waveguide and must be substituted by the appropriate general solutions for $\widetilde{p}(x)$ and $\widetilde{U}(x)$.

An alternate and mathematically identical formulation of the equivalent circuit is the impedance translation expression (ITE). ITEs are closed-form expressions for the input impedance of the waveguide $\widetilde{Z}_B$ in terms of an arbitrary termination impedance $\widetilde{Z}_A$; they are derived by evaluating the general solutions for $\widetilde{p}(x)$ and $\widetilde{U}(x)$ with $\widetilde{Z}_A$ at the $x = L$ end, as follows:

$$\widetilde{Z}_B = \left.\frac{\widetilde{p}(0)}{\widetilde{U}(0)}\right|_{\frac{\widetilde{p}(L)}{\widetilde{U}(L)}\,=\,\widetilde{Z}_A}. \tag{5}$$

Derivations such as these are often included in introductory acoustics texts[11], and we can easily evaluate the above expression to find that the ITE for a straight waveguide is R11

$$\widetilde{Z}_{B,\text{straight}} = \frac{\frac{\rho_0 c}{S}\widetilde{Z}_A + j\frac{\rho_0 c}{S}\tan(kL)}{\frac{\rho_0 c}{S} + j\widetilde{Z}_A\tan(kL),} \tag{6}$$

where $\widetilde{Z}_{B,\text{straight}}$ is the input impedance of the waveguide, and other symbols are as defined previously.

Because the equivalent circuit and ITE above have been derived from the 1D wave equation, they describe the waveguide completely below the cutoff frequency of the cross modes, for arbitrary waveguide length. This is a relaxed requirement compared to the lumped-element approximation and is often an appropriate assumption, as many resonators target low frequencies and are designed to be compact. The straight ITE has been used to model axially symmetric resonators using a discretization of the resonator into many straight segments[12]; this may account for tapers, but it is unclear how accurate the results are in the referenced conference paper. The present approach evaluates tapers separately and is also able to model curved necks. R12

An equivalent circuit for a curved waveguide of constant radius of curvature may be derived from the work of Cummings[13] and of Keefe and Benade[14], who treated curved ducts in the context of musical instruments. Their work sought a characteristic acoustic impedance of a curved duct, analogous to $\rho_0 c/S$ for a straight waveguide. Though they could not solve for sound propagation in a circular curved duct directly, they did find an approximate expression for the characteristic impedance by modeling a circular cross section as a series of rectangular duct slices, each of which could be characterized analytically. These slices were treated as though they were separate ducts in parallel, and by evaluating the inductance and capacitance of these slices, Keefe and Benade[14] found that the curved duct could be treated as a straight duct with a length equal to the mean length of the curved duct, and a characteristic acoustic impedance of the form R13 R14

$$Z_{\text{bend}} = \frac{\rho_0 c}{S}\sqrt{\frac{S}{R_m \int \ln[a(z)]dz}}, \tag{7}$$

where R_m is the mean radius of curvature of the bend, z is the dimension perpendicular to the plane of curvature of the bend, $a(z) = R_o(z)/R_i(z)$ is the ratio of the outer radius of curvature to the inner radius of curvature at a given z, and the integration is performed along the z-extent of the cross section. Expressions for a may be found in Ref. 14 for a circular cross section. The characteristic acoustic impedance of the curved waveguide is therefore equivalent to that of a straight waveguide, multiplied by a geometry-dependent constant. This finding implies that the straight duct expressions Eqns. (4) and (6) may be modified for a curved duct by replacing $\rho_0 c/S$ with Z_{bend} everywhere that it occurs and replacing L with the mean length of the bend, L_m. The modified expressions are given in Eqns. (8) and (9).

$$\begin{aligned}\widetilde{Z}_{1,\text{curved}} &= \widetilde{Z}_{2,\text{curved}} = jZ_{\text{bend}}\tan\left(\frac{kL_m}{2}\right), \\ \widetilde{Z}_{3,\text{curved}} &= -jZ_{\text{bend}}\csc(kL_m)\end{aligned} \tag{8}$$

$$\widetilde{Z}_{B,\text{curved}} = \frac{Z_{\text{bend}}\widetilde{Z}_A + jZ_{\text{bend}}\tan(kL_m)}{Z_{\text{bend}} + j\widetilde{Z}_A\tan(kL_m).} \tag{9}$$

Work by Tang[15] is instructive in deriving expressions for a tapered waveguide. Tang[15] modeled a Helmholtz R15 resonator with a conical tapered neck in 2001, using the Webster horn equation. He did so by first deriving an impedance translation expression for the tapered waveguide, which he then simplified. We can make use of the full expression, which is given here:

$$\widetilde{Z}_{B,\mathrm{tapered}} = \frac{\rho_0 c}{S_B} \frac{\widetilde{Z}_A + \left(j\frac{\rho_0 c}{S_A} - \frac{m}{kr_A}\widetilde{Z}_A\right)\tan(kL)}{\frac{\rho_0 c}{S_A} - j\frac{m^2 L}{kr_A r_B}\widetilde{Z}_A + \left(\frac{\rho_0 c}{S_A}\frac{m}{kr_B} + j\frac{m^2}{k^2 r_A r_B}\widetilde{Z}_A + j\widetilde{Z}_A\right)\tan(kL)}, \tag{10}$$

where r_A and r_B are the radii of the waveguide cross section at the ends corresponding to $\widetilde{Z}_A$ and $\widetilde{Z}_B$, or the $x = L$ end and the $x = 0$ end, respectively; $S_A = \pi r_A^2$ and $S_B = \pi r_B^2$ are the areas of the circular cross sections at each end; and $m = (r_A - r_B)/L$ is the slope of the taper. It is worthwhile to note in the case that the slope is zero the expression collapses to Eqn. (6). In addition to this ITE, equivalent circuits are given here for the conical tapered waveguide. The derivation of these expressions is included in Appendix.

$$\widetilde{Z}_{1,\mathrm{tapered}} = j\frac{\rho_0 c}{S_A}\frac{k^2 r_A r_B\cos(kL) - kr_A\sin(kL) - k^2 r_A^2}{kLm^2\cos(kL) - (m^2 + k^2 r_A r_B)\sin(kL)},$$

$$\widetilde{Z}_{2,\mathrm{tapered}} = j\frac{\rho_0 c}{S_B}\frac{k^2 r_A r_B\cos(kL) - kr_B m\sin(kL) - k^2 r_B^2}{kLm^2\cos(kL) - (m^2 + k^2 r_A r_B)\sin(kL)},$$

$$\widetilde{Z}_{3,\mathrm{tapered}} = j\frac{\rho_0 c}{\pi}\frac{k^2}{kLm^2\cos(kL) - (m^2 + k^2 r_A r_B)\sin(kL)}, \tag{11}$$

where all symbols are defined as in Eqn. (10). While these expressions are visually much more complicated than those in Eqn. (4) or Eqn. (8), they are just as calculable using a computer.

Until now, all impedance formulations have been given solely in terms of the reactive component; for accurate modeling of Helmholtz resonators, resistive losses must also be considered. Duct losses may be accounted for in any of the waveguide models by substituting a complex wavenumber $\widetilde{k}$ for k, as

$$\widetilde{k} = k - j\alpha. \tag{12}$$

R16 For this work, we use the expression for α given in Ref. 16:

$$\alpha = \frac{1}{rc}\sqrt{\frac{\eta ck}{2\rho_0}}\left(1 + \frac{\gamma - 1}{\sqrt{\mathrm{Pr}}}\right), \tag{13}$$

where ρ_0, c, and k are defined as previously, r is the radius of the waveguide, η is the viscosity of the fluid (18.5 μPa · s for air at standard temperature and pressure), γ is the ratio of specific heats (1.4 for air), and Pr is the Prandtl number (0.71 for air). Note that α will typically be different for each waveguide, and thus, each waveguide will have a different complex wavenumber.

2.2 Cavities

In order to create a cavity, or body, for a resonator, one need only terminate a waveguide with an infinite impedance. For the equivalent circuit model, this creates an open circuit, removing the right branch of the T-network. In this work, only a cavity with sides perpendicular to its end is treated, which is derived from setting $\widetilde{Z}_A = \infty$ in Eqn. (6), or by removing the right branch of the T-network in Fig. 1(c). Both methods yield the same result, after simplification, of

$$\widetilde{Z}_{\mathrm{cavity}} = j\frac{\rho_0 c}{S}\cot\left(\widetilde{k}L\right), \tag{14}$$

where S and L are the cross-sectional area and length, respectively, of the cavity. This same procedure applies to cavities created by stopping the end of a curved or tapered waveguide, but these are not investigated in this work.

2.3 End Corrections and Junctions

The complete description of the resonator requires the treatment of the sudden change in cross-sectional area between the neck and body of the resonator. Karal[17] derived expressions for the equivalent impedance of a concentric junction between cylindrical waveguides by expanding both waveguides in terms of cylindrical eigenfunctions. His expression shows that the discontinuity is effectively an added acoustical mass, or inertance. In addition, Bies and Hansen[18] presented an effective resistance of a discontinuity. The impedance may therefore be expressed as R17 R18

$$\widetilde{Z}_{\mathrm{junction}} = j\omega M_{\mathrm{junction}} + R_{\mathrm{junction}}, \tag{15a}$$

with

$$M_{\mathrm{junction}} = \frac{4\rho_0}{\pi r_2}\sum_{m=1}^{\infty}\frac{J_1^2\left(\gamma_m\frac{r_2}{r_1}\right)}{\gamma_m\frac{r_2}{r_1}\left[\gamma_m J_0(\gamma_m)\right]^2}, \tag{15b}$$

where $r_2 < r_1$ are the two radii, $J_n(x)$ is the nth-order Bessel function, and γ_m is the mth zero of the first-order Bessel function, i.e., $J_1(\gamma_m) = 0$, and

$$R_{\text{junction}} = \frac{\rho_0 c}{S_2}\left(0.288kt\log_{10}\left[\frac{4S_2}{\pi h^2}\right] + \frac{S_2 k^2}{2\pi}\right), \quad (15c)$$

where $t = \sqrt{2\eta/\rho_0\omega}$ is the boundary layer thickness, $S_2 = \pi r_2^2$, and h is the larger of t and r_2. For most practical purposes, $h = r_2$; for example, at $\omega = 2\pi$ rad/s in air at standard temperature and pressure, $t \approx 2.2$ mm. $\widetilde{Z}_{\text{junction}}$ as defined in this way describes cylindrical necks and cavities. In addition to cylindrical geometries, the current work reported here has found good empirical agreement for a cylindrical neck attached to a cavity with elliptical cross section by using the semi-major axis of the ellipse in place of a radius in Eqns. (15a)–(15c), as well as in the thermoviscous losses described in Eqn. 13. Typical practice in a lumped-element circuit representation is to approximate the discontinuity as an end correction due to an infinite baffle; Karal[17] showed that the reactive portion of Eqns. (15a)–(15c) approaches this solution as the ratio of radii becomes very large.

In addition to this discontinuity impedance, end corrections are needed for the connection of the resonator neck to the passive noise control environment. These may appropriately include the standard end corrections of a baffled or unbaffled tube, if the mounting conditions so dictate. End corrections for the outer end of the neck will be presented as they are used in the experimental examples.

2.4 Building a Resonator from These Components

With equivalent circuits and impedance translation expressions for each of these resonator components, a full resonator can be built. To illustrate how this is done, consider the resonator depicted in Fig. 2(a). This resonator has a cylindrical cavity, a junction (or discontinuity), and a neck made up of a curved section and a straight section. The equivalent circuit can be built by attaching a terminating cavity impedance in series with the junction impedance to the right end of the curved waveguide network, which is attached to the right end of a straight waveguide network. The full equivalent circuit is shown in Fig. 2(b), where the circuit component expressions would be as given in the preceding sections, evaluated using the physical dimensions of each part of the resonator. Quantities of interest such as the resonator input impedance and pressure and particle velocity at any point in the resonator may be derived from the circuit. If the input impedance of the resonator is the only property of interest, it may be calculated using the ITEs as follows. Adding the cavity and the junction impedance gives the load on the cavity end of the curved waveguide. Using this as $\widetilde{Z}_A$ in Eqn. (9) gives the input impedance at the other end of the curved waveguide $\widetilde{Z}_{B,\text{curved}}$, which also happens to be the load on the deeper end of the straight waveguide. As such, substituting the calculated $\widetilde{Z}_{B,\text{curved}}$ for $\widetilde{Z}_A$ in Eqn. (6) gives the input impedance of the entire resonator, neglecting fluid loading at the mouth for the time being.

Though these formulations do not allow for closed-form expressions for resonator properties, they can easily be implemented in a computer. The authors have implemented an ITE impedance calculation in MATLAB, which is able to calculate impedance over a 6000 Hz bandwidth in under a second on a low-end desktop computer. Comparable calculations for a simple straight-necked resonator with a commercial finite element package took about a factor of two longer to complete. When the additional overhead of preparing meshes for finite element analysis is considered, especially in the context of iterative design, the speed improvements become considerable. In addition, resonance frequencies and Q factors can be gleaned from the calculated impedance curves with very little effort.

2.5 Lumped-Element Impedance Calculation

For comparison, the lumped-element formulation for resonator impedance is given here. The resonator is treated as a series combination of an acoustic mass M_A given by the

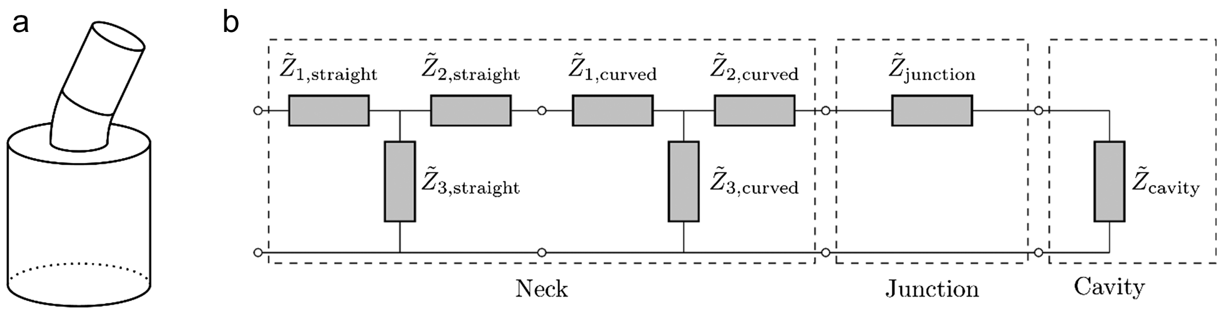

Fig. 2—An example of creating an equivalent circuit for a resonator. (a) A resonator with a cavity, a junction discontinuity, and a two-segment neck. (b) The equivalent circuit of the resonator in (a), where the $\widetilde{Z}$ is defined in the preceding sections.

movement of the air in the neck, an acoustic compliance C_A given by the compression of the air in the body, and an acoustic resistance R_A given by the radiation of the resonator mouth. Damping is introduced using complex frequencies $\widetilde{\omega} = \widetilde{k}/c$, where $\widetilde{k}$ is given by Eqn. (12), with separate complex frequencies calculated for the neck ($\widetilde{\omega}_n$) and the body ($\widetilde{\ }\omega_b$). The impedance is then

$$\widetilde{Z}_{LE} = j\widetilde{\omega}_n M_A + \frac{1}{j\widetilde{\omega}_b} C_A + R_A, \tag{16}$$

where $M_A = \rho_0 L_n / S_n$, $C_A = V/\rho_0 c^2$, $R_A = \rho_0 \omega^2 / 2\pi c$, L_n and S_n are the length and cross-sectional area of the neck, and V is the volume of the resonator body. An end correction appropriate for a resonator mounted in infinite baffle ($\ell_{corr} = 0.85 r_n$) is included in L_n for both ends of the neck unless otherwise specified[19].

The lumped-element formulation does not include provisions for curved or tapered necks, but as an approximation, one may use the average length and cross-sectional area of the complex neck in the expression for M_A. This procedure is what is commonly used in practice when modeling a complex resonator, and it is used to calculate the lumped-element impedances shown in the next section.

3 FABRICATION AND VALIDATION

The foregoing expressions are now validated by comparing predicted impedance to measured impedance of complete resonators containing the various components. Resonators were fabricated using 3D printing to give specific resonance frequencies, as predicted by the equivalent circuits and ITEs. The resonators were mounted on the end of an impedance tube, as shown in Fig. 3, where the impedance was measured using Chung and Blaser's[20] two-microphone method. The impedance tube had an internal radius of 50.8 mm, with an associated cutoff frequency of 1.9 kHz, above which the two-microphone method is inaccurate. Various microphone separation distances were used, and the results were combined, to give valid results over the entire frequency range shown below. The higher-order theory models the discontinuity in cross section between the resonator neck and the impedance tube as a junction discontinuity impedance $\widetilde{Z}_{\text{junction}}$ added in series with the input impedance of the resonator. In addition, the mounting of the resonator to the impedance tube adds a straight segment of 3 mm length to the mouth of the resonator that is not included in resonator dimensions below but is treated in both model predictions.

Fig. 3—The impedance measurement setup, with a resonator attached to the end of an impedance tube. Two microphones are mounted in the impedance tube, and a speaker is mounted on the end opposite the resonator.

Several resonators with various configurations were tested, though only two will be shown here. The first has a straight cylindrical neck and a straight cylindrical body; this resonator is pictured in Fig. 4(b) with dimensions provided in Table 1 and will be referred to as resonator A. The second resonator, resonator B, has a complex neck consisting of a tapered section, a curved section, and a straight section, with a body of elliptical cross section. Resonator B is pictured in Fig. 5(b), and the dimensions are given in Table 2. This resonator requires the assumptions mentioned in Sec. 2.5 in order to evaluate the lumped-element approximation.

Impedance predictions and measurements are compared in Fig. 4(a) for resonator A and in Fig. 5(a) for resonator B. Notice that in both figures the classical impedance calculated by Eqn. (16) only shows one minimum, corresponding to the first resonance, while the higher-order predictions are able to model multiple resonances as well as antiresonances. Resonance predictions are summarized in Table 3. Resonator A is somewhat of a best-case scenario in that the lumped-element impedance calculation has low error in the first resonance frequency. The higher-order theory outperforms the classical theory on both first resonances, however, and is able to represent the entire curves well. For resonator B, we see that the lumped-element predictions for the first resonance are not passably close, as they were for resonator A. Finally, all higher-order predicted resonance frequencies are within 3% of the measured values, with most of them having less than 1% error.

The results seen for these two resonators are representative of what was seen for all the resonators fabricated in this work. Though the lumped-element predictions may have mixed success for simple resonators, the higher-order predictions are consistently accurate. All first resonances were predicted within 1–2 Hz, and the higher resonances had only a few percent error at most. In addition to more accurate resonance predictions, the higher-order theory characterizes the broadband impedance of the resonator, while the lumped-element approximation only approximates the first resonance. These improvements have the potential to better inform passive noise control theories and reduce prototype iteration.

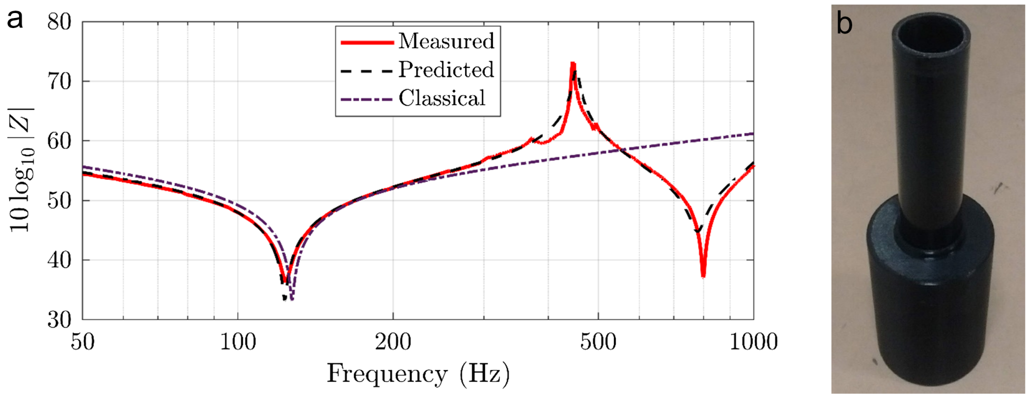

Fig. 4—(a) Impedance measurements and predictions using higher-order and lumped-element theories for resonator A. Resonance occurs at the minimum of impedance. (b) A photograph of the fabricated resonator A.

4 APPLICATIONS

Higher-order predictions of resonator impedance can be utilized in many traditional passive noise control theories to improve accuracy. Many established passive noise control formulations have been developed using a lumped-element model for the resonators, and all of these formulations could potentially benefit from these higher-order predictions. In some of these, the calculated impedance may be substituted directly for the lumped-element impedance; in others, finding the resonance frequency from the impedance curve gives enough information to implement the theory. Some theories are written in terms of lumped elements M_A, C_A, and R_A from Eqn. (16); these can be integrated with the higher-order theory by least-squares fitting Eqn. (16) to the first resonance in the calculated impedance curve. In this article, we give examples of the first two types of integrations to show how this can be done. Predictions of transmission loss due to a resonator side branch are calculated by directly substituting the higher-order resonator impedance into side branch theory. As a second example, coupling between a resonator and an enclosure is achieved using only the resonance frequency of the resonator.

4.1 Side Branch on a Duct

The theory for the transmission loss in a duct due to a lumped-element Helmholtz resonator side branch is closely related to the more general case. It is calculated as

Table 1—Dimensions of resonator A.

	Neck	Body
Radius (mm)	20.125	47.6
Length (mm)	187	147.6

$$\mathrm{TL} = 10\log_{10}\left[1 + \left(\frac{c/2S_{\mathrm{duct}}}{\omega\ell'/S_N - c^2/\omega V_B}\right)^2\right], \qquad (17)$$

where S_{duct} is the cross-sectional area of the duct, S_N is the cross-sectional area of the resonator neck, ℓ' is the effective length of the resonator neck, and V_B is the volume of the resonator body[21]. This expression is derived by substituting the lumped-element impedance of the resonator into the more general expression:

$$\mathrm{TL} = 10\log_{10}\left[\frac{\left|\rho_0 c/2S_{\mathrm{duct}} + \widetilde{Z}_{\mathrm{res}}\right|^2}{\left|\widetilde{Z}_{\mathrm{res}}\right|^2}\right], \qquad (18)$$

where $\widetilde{Z}_{\mathrm{res}}$ is the input impedance of the resonator. Equation (18) is where one can make use of the higher-order predictions: once the resonator input impedance is calculated, it may be substituted into Eqn. (18) to obtain a calculated transmission loss.

This theory using the higher-order impedance predictions was implemented, and the predicted transmission loss was compared to measured results. For this verification, resonators were mounted as a side branch on the duct used for impedance measurements with an anechoic termination added at the end; this setup is shown in Fig. 6. Transmission loss was calculated using the procedure outlined in Refs. 20 and 22, with four microphones measuring the field: two upstream and two downstream of the side branch. This section shows verification of transmission loss predictions using resonator B, though the neck is physically extended 39 mm by the side branch mounting hardware. Because the resonator-duct interface is a curved surface, a specialized end correction is needed. This can be obtained from the work of Ji[23], who found empirically the end correction for a side branch:

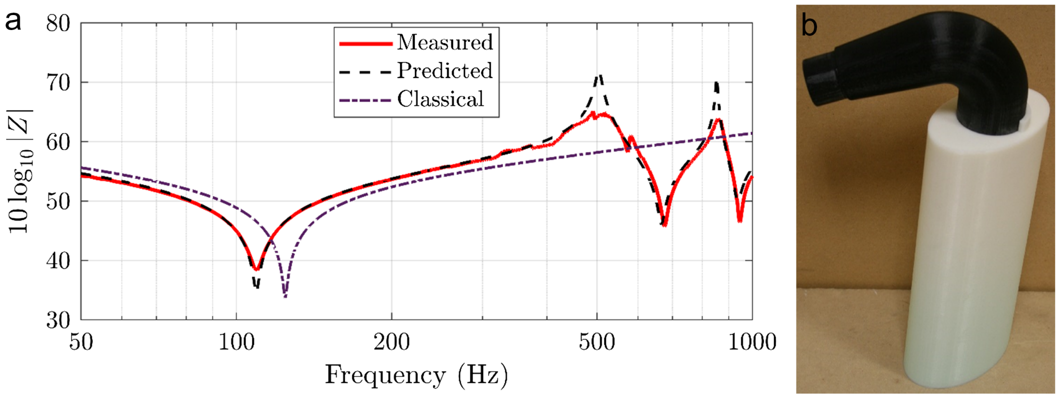

Fig. 5—(a) Impedance measurements and predictions using higher-order and lumped-element theories for resonator B. Resonance occurs at the minimum of impedance. (b) A photograph of the fabricated resonator B.

$$\ell_{0,\mathrm{SB}} = r_m \begin{cases} 0.8216 - 0.0644\xi - 0.694\xi^2 & \xi \le 0.4 \\ 0.9326 - 0.6196\xi & \xi > 0.4 \end{cases}, \quad (19)$$

where r_m is the radius of the side branch mouth and ξ is the ratio of side branch to main duct radii. This end correction is added to the mouth end of the neck as a straight waveguide of length $\ell_{0,\mathrm{SB}}$ for the higher-order predictions and as a replacement for one of the end corrections in the lumped-element neck length. The predicted and measured results for transmission loss are shown in Fig. 7. Like the impedance plots, the measured and predicted frequency of maximum transmission loss matches exactly. The lumped-element prediction is off by 19%.

4.2 Enclosure Mode Coupling

Although the calculated impedance cannot be directly substituted into the resonator-enclosure coupling theory, good coupling predictions can be attained with the extracted resonator properties. In 1980, Fahy and Schofield published a derivation on the resonator-enclosure interaction showing that a Helmholtz resonator tuned to the resonance frequency of an enclosure mode can attenuate that resonance, while creating two coupled resonances at frequencies just above and below the original resonance frequency.[1] These coupled resonances may have higher or lower amplitude than the original resonance, depending on the Q factors of the enclosure and the resonator and the relative volumes of the two. One factor that significantly affects the coupling is how well the resonator is tuned to the resonance of the enclosure. When the resonator is well tuned, the two coupled resonances will have nearly equal amplitude; if the resonator is poorly tuned, one coupled resonance will be much higher in amplitude than the other and will approach the amplitude of the original resonance peak. Tuning the resonator therefore becomes an important step in creating this coupling; this tuning can be achieved before fabrication using the higher- order predictions that have been given here.

An implementation of this passive noise control scenario demonstrated that the higher-order tuning predictions significantly improved the attenuation achieved. Resonator A was coupled to the nearly rectangular plywood enclosure shown in Fig. 8 with a depth of 1.5 m,

Table 2—Dimensions of resonator B, with neck segments listed in order from the outlet of the resonator to the body of the resonator.

Segment:	Tapered	Curved	Straight		Body
Radius (mm)	12.7–20.125	20.125	20.125	Semi major axis (mm)	51.0
Length (mm)	85.0	67.2	22.0	Semi minor axis (mm)	30.4
Bend angle	—	110°	—	Length (mm)	215.8

Table 3—Measured and predicted resonance frequencies for resonators A and B and the percent error of the predictions.

		Resonator A		Resonator B		
	Resonance	First	Second	First	Second	Third
Resonance frequencies (Hz)	Measured	124	799	109	676	946
	Higher order	123.3	778.6	109.3	666.5	937.4
	Lumped element	127.4	—	124.4	—	—
Percent error (%)	Higher order	0.6	2.6	0.3	1.4	0.9
	Lumped element	2.7	—	14.1	—	—

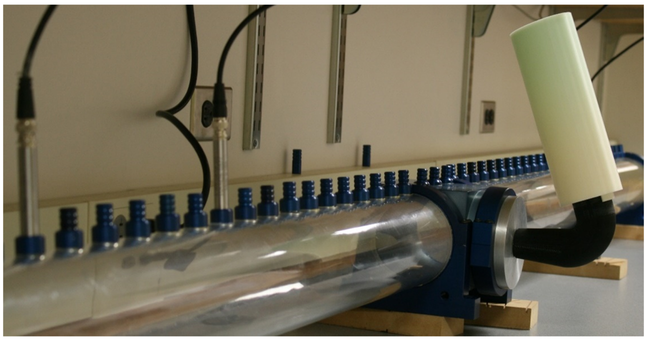

Fig. 6—Test setup for measurement of transmission loss due to resonator B as a side branch.

Fig. 8—Test setup for resonator-enclosure coupling, with resonator A attached to the side of a plywood enclosure.

a height of 0.96 m, and a linearly varying width of 0.99–1.19 m. The response of the (1,0,0) mode to broadband excitation is shown in Fig. 9 as a solid line. Resonator A was fabricated to have a resonance frequency aligned with the center of the full width half max band of this mode at 124 Hz. This fabrication was done twice, with different neck lengths; once so that the higher-order predictions placed the resonance at 124 Hz and again with a slightly longer neck so that the lumped-element predictions placed the resonance at 124 Hz. The resonator was then attached to the enclosure using a hole in the wall where the modal response was a maximum. The infinite baffle end correction, an added neck length of 0.85 times[19] the outlet radius, was used for this mounting scenario.

Figure 9 shows the response of the coupled enclosure-resonator system to broadband noise as the dashed line and the dot-dashed line for the resonator fabricated according to higher-order predictions and lumped-element predictions, respectively. The resonator fabricated according to higher-order predictions achieves an attenuation of 7 dB at the peak frequency, with both coupled resonances having an amplitude more than 3 dB below the original peak. This type of response is typical of a well-tuned resonator. The resonator fabricated according to lumped-element predictions creates a dip in the response at about 118 Hz, which roughly corresponds to the resonance of the resonator. This is a 6 Hz error, or about a 5% relative error, and it causes the resonator to give poor attenuation. One of the coupled resonance peaks is only 1 Hz higher in frequency than the original peak and is only 2 dB lower in amplitude, giving an effective attenuation of about 2 dB. The accuracy of higher-order tuning predictions allows a first-round prototype to achieve 5 dB more attenuation, even in a near-best-case prediction scenario for the lumped-element formula.

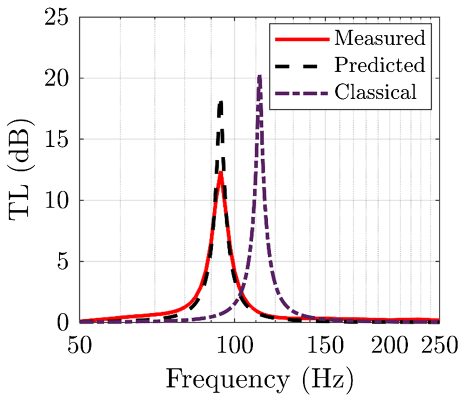

Fig. 7—Transmission loss of resonator B as a side branch on a duct. Solid: measured. Dashed: higher-order predicted. Dot-dashed: classical predicted.

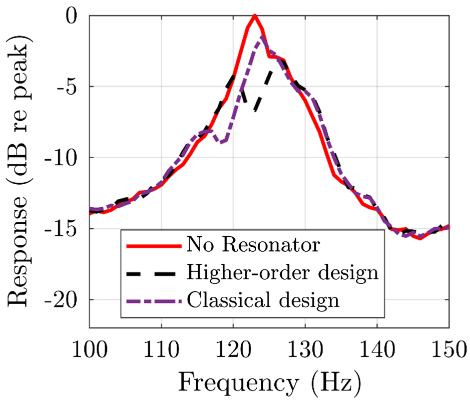

Fig. 9—Response of an enclosure to broadband excitation, with and without resonators. Solid: without a resonator. Dashed: with a resonator fabricated according to higher-order predictions. Dot-dashed: with a resonator fabricated according to lumped-element predictions.

5 CONCLUSIONS

A higher-order model of Helmholtz resonators that can predict resonator properties accurately has been developed. This method uses combinations of one-dimensional solutions to the wave equation and junction impedances to describe complete resonators. Predictions of resonance frequencies have less than 2% error in all cases tested. In addition, the model is quick to evaluate, allowing for rapid calculation of many resonators. This allows the user to investigate numerous possible resonator designs in a short period of time with high confidence that the model will accurately predict the response of the resonator when fabricated. This can be done for a wide variety of resonators, including those with tapered and curved necks, and elliptical bodies.

This article has presented the application of this model to two resonators: a simple concentric cylindrical resonator, and a more complex resonator using a combination of a tapered, curved, and straight neck segments. Both resonators had one-element, straight cavities, but complex cavities with tapers, curves or combinations of the three would also be possible. This theory gives a unified model for Helmholtz resonators and quarter-wave tubes and allows for curved or tapered quarter-wave tubes. In addition, the literature contains studies on other components that could be added, such as end correction when flow is present or exponential tapers. The reader is encouraged to apply similar techniques as those shown here to implement additional components as needed.

This theory allows for higher-order predictions to be implemented in passive noise control theory. Examples of side branch transmission loss and enclosure mode attenuation were shown here, but this can be equally useful for other theories in which lumped-element formulations are traditionally used.

6 ACKNOWLEDGMENTS

The authors gratefully acknowledge Caterpillar, Inc. for their funding and support of this research.

7 APPENDIX: DERIVATION OF THE TAPERED WAVEGUIDE EQUIVALENT CIRCUIT

The Webster horn equation allows for the treatment of waveguides with slowly varying cross section. This differential equation results from the 1D wave equation when the cross-sectional area may vary, and it is written as

$$\frac{1}{S(x)}\frac{d}{dx}\left(S(x)\frac{d\widetilde{p}}{dx}\right) + k^2\widetilde{p} = 0, \qquad \text{(A1)}$$

where $S(x)$ is the varying cross-sectional area, $\widetilde{p}$ is the acoustic pressure, k is the wavenumber, and x is the dimension along the waveguide. If conical spreading is assumed, $S(x) = \pi(r_B + mx)^2$, where $m = (r_A - r_B)/L$ is the slope of the taper, and r_A and r_B are the radii at the right and left ends, respectively, of the taper. By substituting and simplifying, the general solution for the pressure may be found[16] to be

$$\widetilde{p}(x) = \frac{m}{k(mx + r_B)}\left(C_1 e^{-jk(mx+r_B)/m} + C_2 e^{jk(mx+r_B)/m}\right), \qquad \text{(A2)}$$

where C_1 and C_2 are arbitrary constants to be determined. The general solution for the volume velocity can be found from Eqn. (A2) using Euler's equation and (substituting $\alpha = mx + r_B$) is

$$\begin{aligned}\widetilde{U}(x) &= j\frac{S(x)}{\rho_0\omega}\frac{d\widetilde{p}}{dx} \\ &= \frac{m\pi}{\rho_0\omega k}\left(C_1(k\alpha - jm)e^{-jk\alpha/m} - C_2(k\alpha + jm)e^{jk\alpha/m}\right),\end{aligned} \qquad \text{(A3)}$$

where ρ_0 is the density of air and ω is the angular frequency. Finally, by substituting Eqns. (A2) and (A3) into Eqns. (3a)–(3c) and simplifying, it is found that

$$\widetilde{Z}_{1,\text{tapered}} = j\frac{\rho_0 c}{S_A}\,\frac{k^2 r_A r_B\cos(kL) - kr_A\sin(kL) - k^2 r_A^2}{kLm^2\cos(kL) - (m^2 + k^2 r_A r_B)\sin(kL)},$$

$$\widetilde{Z}_{2,\text{tapered}} = j\frac{\rho_0 c}{S_B}\,\frac{k^2 r_A r_B\cos(kL) - kr_B m\sin(kL) - k^2 r_B^2}{kLm^2\cos(kL) - (m^2 + k^2 r_A r_B)\sin(kL)},$$

$$\widetilde{Z}_{3,\text{tapered}} = j\frac{\rho_0 c}{\pi}\,\frac{k^2}{kLm^2\cos(kL) - (m^2 + k^2 r_A r_B)\sin(kL)}, \qquad \text{(A4)}$$

which are equivalent to Eqns. (11a)–(11c).

8 REFERENCES

1. F.J. Fahy and C. Schofield, "A note on the interaction between a Helmholtz resonator and a mode of an enclosure", *J. Sound Vib.*, **72**(3), 365–378, (1980).
2. Q. Mao and P. Stanislaw, "Control of sound transmission through double wall partitions using optimally tuned Helmholtz resonators", *Acta Acustica united with Acustica*, **91**(4), 723–731, (2005).
3. M. Alster, "Improved calculation of resonant frequencies of Helmholtz resonators", *J. Sound Vib.*, **24**(1), 63–85, (1972).
4. J.W. Strutt, "V. On the theory of resonance", *Phil. Trans. R. Soc. Lond.*, **161**, 77–118, (1871).
5. K. Ingard, "On the radiation of sound into a circular tube, with an application to resonators", *J. Acoust. Soc. Am.*, **20**, 665–682, (1948).
6. K. Ingard, "On the theory and design of acoustic resonators", *J. Acoust. Soc. Am.*, **25**, 1037–1061, (1953).
7. N. Dickey and A. Selamet, "Helmholtz resonators: one-dimensional limit for small cavity length-to-diameter ratios", *J. Sound Vib.*, **195**, 512–517, (1996).

8. L.L. Beranekand T.J. Mellow, "Electro-mechano-acoustical circuits", in *Acoustics: Sound Fields and Transducers*, edited by L. L. Beranekand T. J. Mellow (Academic Press, Massachusetts, 2012), vol. **chap. 3**.
9. J.L. Flanagan, "Acoustical properties of the vocal system", in *Speech Analysis Synthesis and Perception*, edited by J. L. Flanagan (Springer-Verlag, New York, 1972), vol. **chap. 3**.
10. H.H. Skilling, "Solution of network equations", in *Electrical Engineering Circuits*, edited by H. H. Skilling (John Wiley & Sons, New York, 1965), vol. **chap. 9**.
11. L.E. Kinsler, A.R. Frey, A.B. Coppensand J.V. Sanders, *Fundamentals of Acoustics* (John Wiley and Sons, 1999), pp. 273.
12. T. Iwase, S. Sugie, H. Kurono, M. Abe, Y. Okadaand K. Yoshihisa, "Sound absorption characteristic of glass and plastic bottles: considerations of their dependences on material properties", *ASME2018 at InterNoise2018* (2018).
13. A. Cummings, "Sound transmission in curved duct bends", *J. Sound Vib.*, **45**, 91–104, (1976).
14. D.H. Keefe and A.H. Benade, "Wave propagation in strongly curved ducts", *J. Acoust. Soc. Am.*, **74**, 330–332, (1983).
15. S.K. Tang, "On Helmholtz resonators with tapered necks", *J. Sound Vib.*, **279**, 1085–1096, (2005).
16. L.E. Kinsler, A.R. Frey, A.B. Coppens, and J.V. Sanders, *Fundamentals of Acoustics* (John Wiley and Sons, 1999), pp. 230–234, 277–280.
17. F. Karal, "The analogous acoustical impedance for discontinuities and constrictions of circular cross section", *J. Acoust. Soc. Am.*, **25**, 327–334, (1953).
18. D.A. Biesand C.H. Hansen, *Engineering Noise Control—Theory and Practice* (Taylor and Francis, New York, 2009), pp. 443.
19. P.M. Morse, *Vibration and Sound* (Acoustical Society of America, New York, 1981), pp. 247–248.
20. J.Y. Chung and D.A. Blaser, "Transfer function method of measuring in-duct acoustic properties. I. Theory", *J. Acoust. Soc. Am.*, **68**(3), 907–913, (1980).
21. L.E. Kinsler, A.R. Frey, A.B. Coppensand J.V. Sanders, *Fundamentals of Acoustics* (John Wiley and Sons, 1999), pp. 288–296.
22. Standard Test Method for Normal Incidence Determination of Porous Material Acoustical Properties Based on the Transfer Matrix Method, International Standard ASTM E2611-17 (ASTM International, West Conshohocken, PA, 2017).
23. Z.L. Ji, "Acoustic length correction of closed cylindrical side-branched tube", *J. Sound Vib.*, **283**, 1180–1186, (2005).

Author Query Form

Journal: NCE

Article: nce67606

Query No.	Query	Remark
Q1	Citation “Eqn. (15)” in the text has been changed to “Eqns. (15a)–(15c)” to match the equations in the text. Please check if this is appropriate.	
Q2	Reference citations in the text were not in sequence and thus renumbered. Please check.	
Q3	Please provide publisher's location for Ref. 11.	
Q4	Please provide publisher's location for Ref. 16.	
Q5	Please provide publisher's location for Ref. 21.	